THE JOURNAL OF PHYSICAL CHEMISTRY A
A JOURNAL OF THE AMERICAN CHEMICAL SOCIETY

pubs.acs.org/JPCA Article

Low-Energy Electron Interactions with Resveratrol and Resorcinol: Anion States and Likely Dissociation Pathways

Ely G. F. de Miranda, Lucas M. Cornetta, and Márcio T. do N. Varella*

Cite This: J. Phys. Chem. A 2022, 126, 7667−7674 Read Online

ACCESS | Metrics & More | Article Recommendations | Supporting Information

ABSTRACT: We report a computational study of the anion states of the resveratrol (RV) and resorcinol (RS) molecules, also investigating dissociative electron attachment (DEA) pathways. RV has well-known beneficial effects in human health, and its antioxidant activity was previously associated with DEA reactions producing H_2. Our calculations indicate a valence bound state (π_1^*) and four resonances (π_2^* to π_5^*) for that system. While the computed thermodynamic thresholds are compatible with DEA reactions producing H_2 at 0 eV, the well-known mechanism involving vibrational Feshbach resonances built on a dipole bound state should not be present in RV. Our results suggest that the shallow π_1^* valence bound state is expected to account for H_2 elimination, probably involving π_1^*/σ_{OH}^* couplings along the vibration dynamics. The RS molecule is also an oxidant and a subunit of RV. Because two close-lying hydroxyl groups are found in the RS moiety, the H_2-elimination reaction in RV should take place at the RS site. Our calculations point out a correspondence between the anion states of RV and RS and even between the thresholds. Nevertheless, the absence of bound anion states in RS, indicated by our calculations, is expected to suppress the H_2-formation channel at 0 eV. One is led to conclude that the ethene and phenol subunits in RV stabilize the π_1^* state, thus switching on the DEA mechanism producing H_2.

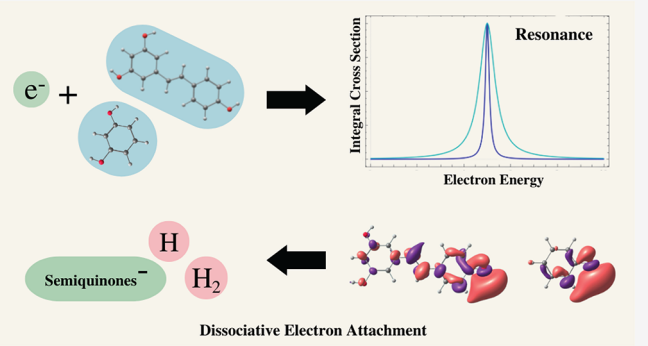

INTRODUCTION

Life on our planet relies on two fundamental processes: respiration and photosynthesis. They provide the means for the cellular energy production which is necessary for the living organisms.[1] Both processes are inseparably linked with the presence of electrons moving through biological matter.[2] This balance is fulfilled along electron transfer pathways, in particular the mitochondrial electron transport chains (ETCs).[3] However, reactive oxygen species (ROS), which are also produced along the mitochondrial ETC, are efficient oxidative substances capable of damaging the mithocondrial membranes, attacking DNA, and causing mutations.[4] Molecular oxygen reduction generates the anionic superoxide, $O_2 + e^- \rightarrow O_2^{\bullet -}$, which can give rise to oxidative stress[5] leading to pathologies such as cardiovascular diseases, Alzheimer's, and Parkison's.[6,7] Nonetheless, ROS can also be beneficial to the cell, e.g., by producing oxidative damage to pathologies and taking part in cellular signaling.[5] Protective mechanisms that neutralize ROS are linked with the generation of native antioxidants or enzymatic activity. Oxireductive balance perturbations in mithocondrial intermembrane space are therefore believed to trigger significant cellular damage.[8]

Polyphenolic antioxidants, such as flavonoids and spinochromes, are good electron acceptors and can interact with electrons under reductive conditions in cells.[9] Dissociative electron attachment (DEA) to multiple OH-substituted aromatic compounds has been found to produce neutral H_2,[9] which is an antioxidant species used clinically.[10] These facts suggest that the antioxidant activity of polyphenolic compounds could be related to the electron-induced production of molecular hydrogen. The xenobiotic antioxidant compounds could be reduced in the mitochondrial intermembrane space by charge leaking from the ETC. The reduction can be viewed as the formation of transient negative ions (TNIs), also called resonances, that can initiate DEA reactions producing H_2 among other species. These mechanisms have been proposed to underlie the antioxidant activity of the polyphenolic compound resveratrol (RV)[11] and also the antipsoriatic activity of anthralin.[12]

The RV molecule (3,5,4′-trihydroxystilbene, shown in Figure 1) is a naturally occurring plant phytoalexin and a

Received: August 12, 2022
Revised: September 21, 2022
Published: October 17, 2022

https://doi.org/10.1021/acs.jpca.2c05789
J. Phys. Chem. A 2022, 126, 7667−7674

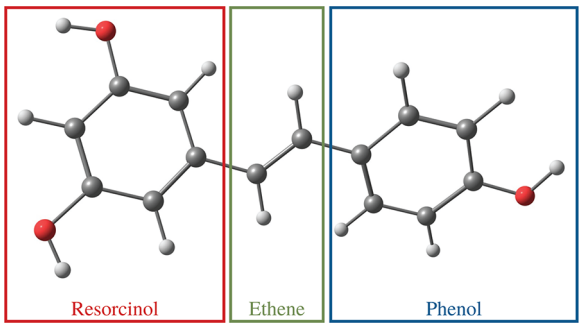

Figure 1. Structure of the resveratrol molecule, with the oxygen atoms indicated in red, carbon in gray, and hydrogen in white. The resorcinol, ethene, and phenol subunits are highlighted.

constituent of red wine. It is known for its strong antioxidant activity[13] and produces beneficial effects in human health by preventing a variety of illnesses, such as cancer, cardiovascular malfunction, neurodegenerative diseases, inflammation, and atherosclerosis.[13] The mechanisms underlying those beneficial effects are not yet clear. Because H and H_2 can be produced by DEA to RV, we presently investigate the TNIs employing electron scattering calculations, and we also infer the possible dissociation pathways. A major difficulty to model the transient anion states of RV is the computational effort arising from the system size and lack of symmetry elements. The RV molecule has 29 atoms and can be considered large for scattering calculations. However, RV can be decomposed into resorcinol (RS), ethene, and phenol (Ph) subunits, as indicated in Figure 1. The smaller subunits have been the subject of previous studies,[14,15] so we presently consider RS, which is also an antioxidant.[16,17] In view of the two hydroxyl groups lying at meta positions with respect to each other in RS, H_2-elimination reactions in RV are likely to take place at the RS moiety. To this extent, the smaller RS molecule could be a more suitable prototype for the DEA reaction producing molecular hydrogen, justifying the study of both the RS and RV molecules. We therefore investigate the bound and transient anion states of those molecules, as well as the thermodynamical thresholds, to infer the DEA mechanisms for H- and H_2-elimination reactions.

This paper is organized as follows. In Computational Procedures we present the theoretical and computational methods for scattering calculations (Schwinger multichannel method with pseudopotentials) employed for the anions characterizations. In the Results and Discussion sections we present the calculations and discuss our findings. Finally, our findings are summarized in the Conclusions scetion.

COMPUTATIONAL PROCEDURES

All scattering calculations were performed in the fixed-nuclei approximation. Equilibrium geometries and vibrational analysis for the neutral molecules were performed with density functional theory (DFT), employing the ωB97XD functional and the 6-311++G(d,p) basis set, as implemented in the Gaussian09 package.[18] Three planar conformers were identified for the RS molecule, differing by the orientation of the hydroxyl groups, as shown in Figure 2. The conformers (b) and (c) belong to the C_{2v} symmetry point group, while the conformer (a) belongs to the C_s group. On the basis of the free energies at room temperature ($k_BT \approx 26$ meV), we assign the conformer (b) as the most stable one, lying 2 and 28 meV below the (a) and (c) forms, respectively. Therefore, an admixture of the three conformers should be present in gas-phase experiments justifying scattering calculations for all of them. In contrast to the small differences in the free energy values, the dipole moment magnitudes are significantly affected by the orientation of the hydroxyl groups. We obtained $\mu = 1.4$ D for the optimal structure (a) versus $\mu = 2.5$ D and $\mu = 2.3$ D for conformers (b) and (c), respectively.

For the RV molecule, the existence of cis (c-RV) and trans (t-RV) isomers deserves a closer look. The relative ground state energies of the RV isomers, also calculated with the ωB97XD/6-311++G(d,p) method, indicate that the t-RV isomer is significantly more stable than the cis counterpart by 0.3 eV. While the geometries of the cis and trans isomers are shown in Figure 3, we no longer consider the cis form in view of the negligible Boltzmann populations. The geometry of the t-RV isomer was somewhat sensitive to the choice of the

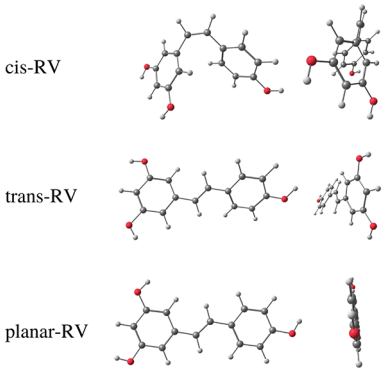

Figure 3. Structures of the RV molecule computed with the ωB97XD/6-311++G(d,p) method (front and side views). The oxygen atoms are represented in red color, carbon in gray, and hydrogen in white.

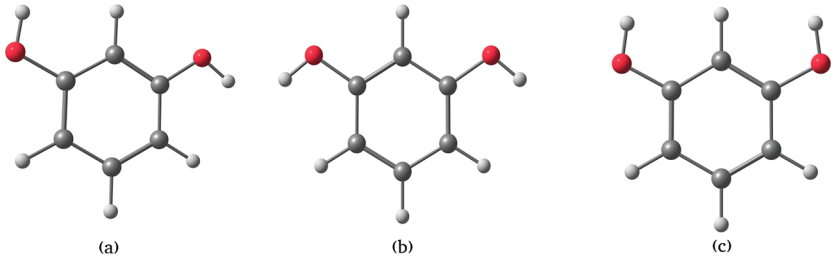

Figure 2. Planar conformers of the resorcinol molecule, labeled (a) to (c). The oxygen atoms are indcated in red, carbon in gray, and hydrogen in white.

https://doi.org/10.1021/acs.jpca.2c05789
J. Phys. Chem. A 2022, 126, 7667−7674

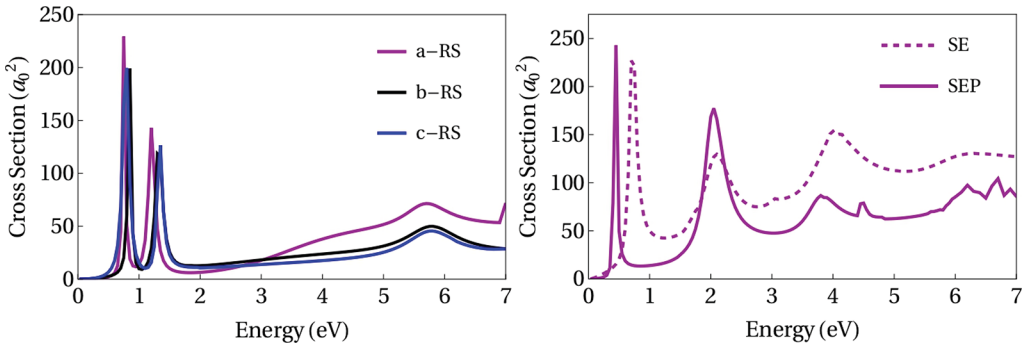

Figure 4. Left panel: integral cross section for elastic electron scattering by a-RS (magenta line), b-RS (black line), and c-RS (blue line). The results correspond to the (A_2 + B_1) symmetry components for b-RS and c-RS, while A″ for a-RS. Right panel: A′′ integral cross section for p-RV calculated in the SE (dashed line) and SEP (solid line) approximations.

exchange-correlation functional. The ωB97XD/6-311++G-(d,p) calculations predict a torsion angle between the aromatic rings around 15° (see Table S1). However, exploratory optimizations performed with the B3LYP/6-311++G(d,p) method indicate a smaller angle, around 4°, in agreement with previously reported DFT/B3LYP results.[11] Because dispersion interactions are accounted for in the ωB97XD functional, although not in B3LYP, the discrepancy in the torsion angle suggests that the interaction between the unsaturated rings would not be accurately described without dispersion corrections.[19,20] For the RS conformers, not having inter-ring $\pi-\pi$ interactions, the B3LYP and ωB97XD functionals predict similar structures.

Despite the deviation from planarity arising from the torsion angle, the scattering calculations employed a planarized geometry of the t-RV isomer, termed p-RV (also computed with the ωB97XD/6-311++G(d,p) method, see Figure 3). Previous scattering studies of nucleobases[21−23] used a similar procedure because the planar structures allow for symmetry decomposition which reduces the computational effort. In addition, the signatures of the shape resonances become more evident in the symmetry-decomposed calculated cross sections. We estimated errors around 0.1 eV between t- and p-RV resonance positions employing empirically corrected virtual orbital energies, according to Scheer and Burrow.[24]

The scattering cross sections were computed with the parallel version of the Schwinger multichannel method implemented with the Bachelet−Hamann−Schlüter (BHS) pseudopotentials (SMCPP).[25,26] The method was recently reviewed,[27] so we briefly outline a few relevant aspects. The scattering electronic wave function is given by

$$|\Psi_{\mathbf{k}_i}^{(\pm)}\rangle = \sum_{\mu} c_{\mu}^{(\pm)}(\mathbf{k}_i)|\chi_{\mu}\rangle \tag{1}$$

where $\mathbf{k}_i$ denotes the wave vector of the incident electron and + (−) stands for the boundary condition associated with outgoing (incoming) spherical waves.[28] The method uses square-integrable functions to build the trial set $\{\chi_\mu\}$, which is very convenient from the computational point of view. The basis vectors $|\chi_\mu\rangle$ are termed configuration state functions (CSFs) and correspond to spin-adapted (N + 1)-particle Slater determinants built on the closed-shell ground state of the neutral target, comprising N electrons. The latter reference state is described at the restricted Hartree−Fock (RHF) level, employing sets of Cartesian Gaussian basis functions. The 5s5p2d basis sets described by Bettega et al.[26,29] were used for the carbon and oxygen atoms, while the 4s basis set reported by Dunning[30] was used for the hydrogens, amounting to a total of 274 basis functions for each RS structure and 580 for the p-RV structure. The RHF calculations were performed with the GAMESS package.[31]

The scattering calculations were restricted to the elastic channel, which is a reasonable approximation for electron energies below the excitation threshold. Two models were explored to construct the CSF space. In the static-exchange (SE) approximation, the target is kept frozen in the ground state $|\Phi_0\rangle$, while the unoccupied (virtual) orbitals are used as scattering orbitals $|\phi_m\rangle$, i.e., $|\chi_m\rangle = \mathcal{A}_{N+1}|\Phi_0\rangle \otimes |\phi_m\rangle$, where $\mathcal{A}_{N+1}$ is the antisymmetrization operator. This approximation does not recover the response of the target electrons to the incoming electron. Even though the SE approach retrieves the physics of shape resonances, at lower energies the dynamical response of the target electrons, termed correlation-polarization effects, should be accounted for. In the static-exchange plus polarization (SEP) approximation, virtual excitations of the target are allowed, so the CSF space is augmented with configurations of the type $|\chi_{\text{im}}\rangle = \mathcal{A}_{N+1}|\Phi_i\rangle \otimes |\phi_m\rangle$, in which $|\Phi_i\rangle$ represents a singly excitation of the target and $|\phi_m\rangle$ is a scattering orbital. In this approximation, long-range polarization (induced dipole moment) and short-range correlation are taken into account. The SEP functions require the choice of three orbitals, two of which are associated with the excitation of the target (hole and particle) and the third being the scattering orbital. The CSF space is built according to the energy criterion proposed by Kossoski and Bettega.[32] All single-particle orbitals whose energy eigenvalues satisfy $\epsilon_{\text{scat}} + \epsilon_{\text{part}} - \epsilon_{\text{hole}} < \Delta$ are taken into account, where ϵ_{scat}, ϵ_{part}, and ϵ_{hole} are the energies of the scattering, particle, and hole orbitals, respectively, while Δ is a cutoff. Finally, modified virtual orbitals (MVOs)[33] were used as particle and scattering orbitals. They were generated from cationic Fock operators with charge +6 for RS and +8 for RV.

The integral cross sections (ICSs) of a-RS and p-RV were decomposed into the A′ and A″ components of the C_s group, while for the b-RS and c-RS the ICSs are decomposed into the four components of the C_{2v} group, namely A_1, A_2, B_1, and B_2. In the SEP approximation for a-RS, we employed Δ = −0.95 hartree for the A′ and A″ components, generating 15405 and 15228 configurations. Similarly, for b-RS (c-RS), we employed Δ = −0.85 hartree for the A_1 component, resulting in 9978 (10053) configurations, and Δ = −1.00 hartree for A_2, B_1, and B_2 components, resulting in 6619 (6633), 6682 (6724), and

https://doi.org/10.1021/acs.jpca.2c05789
J. Phys. Chem. A 2022, 126, 7667−7674

6654 (6654) configurations, respectively. For the case of p-RV, only the A″ component was considered because we do not expect resonance signatures in the A′ ICS component. In this case, we employed Δ = −0.95 hartree, resulting in 17969 CFSs.

While only elastic collisions were taken into account, some insight into the inelastic channels can be gained from bound state calculations. The lowest lying excited states of the neutral RS molecule were explored with the CASPT2 method.[34] These calculations were performed with the OpenMOLCAS software,[35] and the active space is described in the Supporting Information. Finally, DEA reaction thresholds were estimated with the composite G4(MP2) method,[36] as implemented in the Gaussian09 package. The thresholds were estimated as the difference between the G4(MP2) energies of products, including the anionic fragment, with respect to the energy of the neutral reactant (see the Discussion section).

RESULTS

As expected, only π^* resonances have clear signatures in the calculated ICSs, for both RV and RS. The corresponding peaks appear in the A_2 and B_1 components of C_{2v} molecules (b- and c-RS) while in the A″ component of C_s molecules (a-RS and p-RV). It is worth noting that C_s is a subgroup of C_{2v}, so the sum of the A_2 and B_1 components correspond to A″. In the left panel of Figure 4, we show the SEP-level ICSs obtained for a-RS (A″ component) as well as b-RS and c-RS (A_2+B_1 components). We observed three π^* shape resonances for all geometries. These are labeled π_1^* to π_3^*, in order of increasing energy, according to the virtual orbitals that accommodate the additional electron. Respectively for a-, b-, and c-RS, the anion states are located at 0.75, 0.84, and 0.78 eV (π_1^*); 1.21, 1.33, and 1.34 eV (π_2^*); and 5.70, 5.79, and 5.78 eV (π_3^*). In general, the positions of the π^* resonances are similar for the three conformers. The excitation threshold of the first excited state of the target molecule was estimated as ≈3.9 eV for all isomers, indicating that the π_3^* resonance might have a mixed shape and core-excited character.

The SMCPP method allows for the diagonalization of the scattering Hamiltonian represented in the square-integrable CSF basis. This procedure generates a set of pseudostates because the actual spectrum is not discrete, but it provides insight into the resonance orbitals. The orbital plots shown in Figure 5 were obtained from the SEP approximation pseudo-eigenstates, although projecting them on the SE subspace. The properly renormalized projections of the eigenstates can be recast as linear combinations of the MVOs, which represent the resonant orbital (occupied by the attached projectile). Even though we only show orbitals for the c-RS structure, similar results were obtained for the other RS isomers. The calculated positions and widths of the resonance states are summarized in Table 1. The SEP approximation results for the RS isomers are similar, except for the width of the π_1^* anion state. The 50 meV difference can nevertheless be viewed as small in absolute value. The widths were obtained from standard local-approximation fits of Breit−Wigner profiles to the calculated eigenphase sums, so the origin of the discrepancy is unclear.

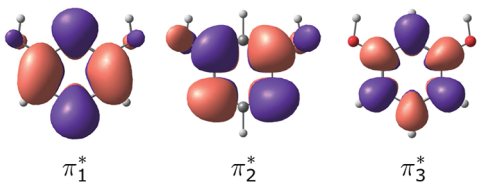

Figure 5. π^* type orbitals of RS obtained from the pseudo-eigenstates of the scattering Hamiltonian. The orbitals are linear combinations of the MVOs employed in the scattering calculations.

The right panel of Figure 4 shows the A″ component of the ICS for p-RV. The SE calculations point out five π^* shape resonances around 0.72 eV (π_1^*), 2.09 eV (π_2^*), 4.02 eV (π_3^*), 6.10 eV (π_4^*), and 10.24 eV (π_5^*). The latter anion state lies outside the energy range employed in Figure 4, for clarity (see also Table 1). The interpretation of the SEP results for this system turned out to be more difficult because we only identified three π^* shape resonances at 0.44, 2.05, and 3.81 eV. The SEP spectrum could be clarified by inspecting the pseudo-eigenstates of the scattering Hamiltonian, as described above. The lowest-lying π_1^* state becomes bound with respect to the neutral molecule by 70 meV, in consistency with previous results.[11] The 0.44 eV peak can be assigned to the π_2^* resonance, while the π_3^* and π_4^* states merge into a single peak around 2.05 eV. The overlap between these resonances explains the apparently absent peak in the SEP results. Lastly, the signature of the π_5^* state, expected to have mixed character, is found around 3.8 eV. In general, a balanced description of polarization effects among several resonances belonging to the same irreducible representation is a challenging task in SEP calculations. Because there are five anion states in the A″ symmetry component of RV, our SEP results might not be properly balanced. It should be clear that going beyond the SEP approximation for a system as large as RV would not be a trivial computational task. The π^* orbital plots obtained from the SEP approximation pseudo-eigenstates projected on the SE space are shown in Figure 6.

DISCUSSION

DEA to RV was investigated experimentally.[8,11] While the target molecules were evaporated at 170 °C, and the collision cell was kept at 180 °C to avoid condensation, the c-RV isomer is not expected to have a significant Boltzmann population, as discussed above. The main fragments observed in the energy- and mass-resolved measurements are summarized in Table 2 along with the peak energies and relative intensities. The calculated energy of the π_2^* state, 0.44 eV, is compatible with the DEA peak for the elimination of two hydrogens (0.6 eV). The nearly degenerate resonances, π_3^* and π_4^*, are expected to give rise to the most intense DEA signal (1.2 eV), corresponding to the H-elimination reaction. The disagreement in energy is another indication that our scattering calculations overestimate the resonances positions (2.0 eV). Finally, the DEA peaks around 4 eV are compatible with the π_5^* resonance, which was predicted at 3.8 eV (SMCPP). In this case the SMCPP result seems in better agreement with the data, but it could be to some extent fortuitous because core-excited anion states may account for the signal around 4.0 eV, at least partly. The abstraction of H atoms mediated by π^* resonances should also involve σ^* anion states with antibonding character on the polar OH groups. Those resonances typically do not have clear signatures in the

https://doi.org/10.1021/acs.jpca.2c05789
J. Phys. Chem. A 2022, 126, 7667−7674

Table 1. Resonance Positions and Widths (Given in Parentheses), in Units of eV, for a-, b-, and c-RS as Well as p-RV[a]

system	π_1^*	π_2^*	π_3^*	π_4^*	π_5^*
a-RS	0.75 (0.05)	1.21 (0.12)	5.70 (0.91)		
b-RS	0.84 (0.06)	1.33 (0.13)	5.79 (1.02)		
c-RS	0.78 (0.11)	1.34 (0.11)	5.78 (1.02)		
p-RV (SE)	0.72 (0.13)	2.09 (0.54)	4.02 (0.91)	6.10 (2.12)	10.24 (2.46)
p-RV (SEP)	−0.07	0.44 (0.05)	2.05 (0.39)	2.05 (0.39)	3.81 (0.56)

[a]SEP results are reported for RS, while SE and SEP for RV. The negative energy value indicates a bound state of the anion.

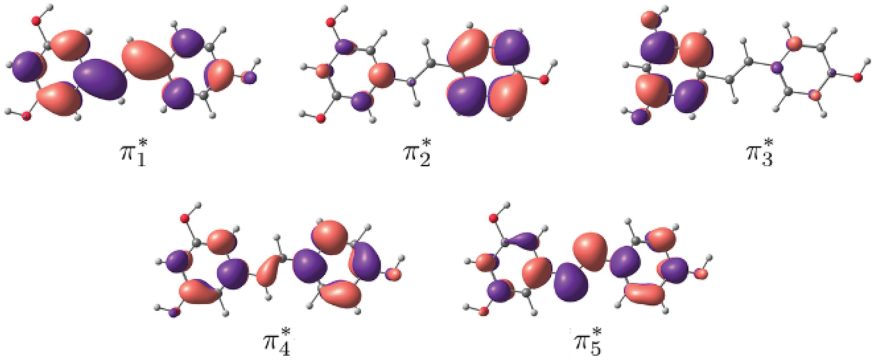

Figure 6. p-RV π^*-type orbitals obtained from the pseudo-eigenstates of the scattering Hamiltonian. The orbitals are linear combinations of the MVOs employed in the scattering calculations.

Table 2. Anion Fragments Observed in DEA Experiments[11,a]

fragment	energy	intensity
M^-	0.0	45
$[M-H]^-$	1.2	100
	4.3	24
$[M-2H]^-$	0.0	17
	0.6	*
$[M-3H]^-$	4.5	0.8
	9.5	1.3
$[M-(CH)_2OH]^-$	8.7	0.8

[a]The fragments, peak energies (in eV), and relative intensities are shown (the asterisk indicates a low intensity).

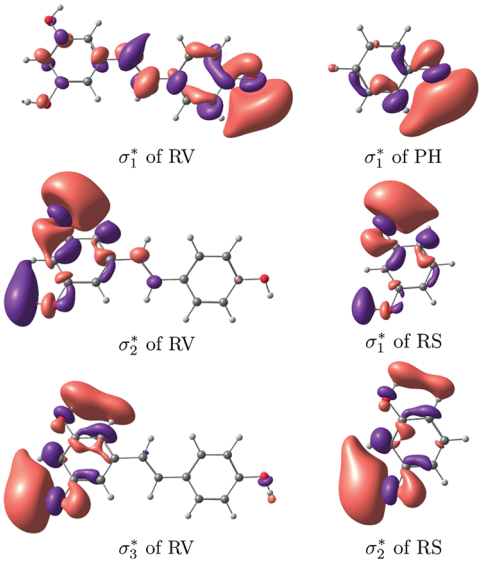

Figure 7. σ^* virtual orbitals obtained with the ωB97XD/6-31G* for the RV, RS, and Ph molecules.

scattering cross sections,[25,37,38] although indirect evidence can be provided by virtual orbitals calculated with compact basis sets. As shown in Figure 7, we could find antibonding virtual orbitals with σ_{OH}^* character and similar amplitudes in the Ph and RS subunits of the RV molecule.

Turning our attention to the DEA signals at 0 eV, one should recall that the dipole moment of the RV molecule can exceed 3.0 D in case the hydroxyl groups in the RS subunit are properly aligned, as shown in Figure 8. We employed the aug-cc-pVDZ basis set augmented with a 6s6p set of diffuse functions, as suggested by Skurski et al.,[39] to survey dipole-supported states in the RV conformers. We could only converge a DBS for the most strongly polar form (μ = 3.3 D). The binding energy obtained at the MP2 level was very small, below 1 meV. Even if the DBS exists at all, we believe the well-known mechanism for H elimination,[40] initiated by vibrational Feshbach resonances (VFRs) built on a DBS, would not account for the 0 eV signal in RV. According to our ωB97XD/6-311++G(d,p) calculations, the ground state of neutral RV has three OH stretch modes with energies close to 3920 cm^{-1} (0.49 eV). In view of the nearly zero binding energy of the DBS, the ν_{OH} = 1 VFRs would lie significantly above the observed DEA peak, around 0.5 eV. In addition, the orientation of the dipole vector in the most strongly polar conformer favors H elimination from the Ph subunit, such that the formation of molecular hydrogen would be unlikely. The direction of the dipole moment favors H_2 elimination in a less polar conformation (μ = 2.3 D, see Figure 8), but we could not obtain a DBS for this conformer.

As mentioned above, the diagonalization of the scattering Hamiltonian indicates a bound π_1^* state for the p-RV geometry. This result is confirmed by ωB97XD/6-311++G(d,p) calculations for t-RV (binding energy of 50 meV), although not by the B3LYP/6-311++G(d,p) calculations. Because the DEA data at 0 eV is compatible with the existence of a bound anion state, we believe the shallow π_1^* state should

https://doi.org/10.1021/acs.jpca.2c05789
J. Phys. Chem. A 2022, 126, 7667−7674

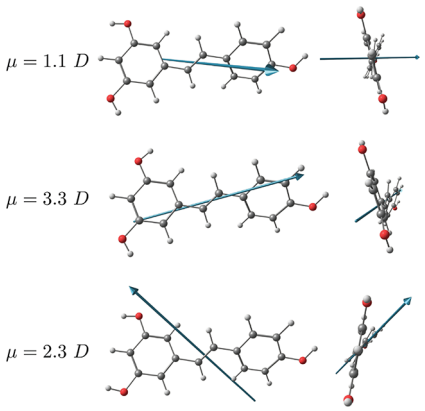

Figure 8. Dipole moment vector and magnitude of the three RV isomers calculated with ωB97XD/6-311++G(d,p).

account for the low-energy DEA signals. The binding energy (≈50 meV) is rather close to the thermal energy under experimental conditions (k_BT = 39 meV), such that VFRs at 0 eV can arise from low-energy vibrational modes, ranging from ∼0 to ∼50 meV. Relaxation of the π_1^* state is favored by the dense vibrational spectrum, in consistency with the observation of the parent M^- anion at 0 eV. Even though the pathway for H_2 elimination is not evident, it should involve π_1^*/σ_{OH}^* couplings along the vibration dynamics.

The calculated reaction thresholds for the H- and H_2-elimination channels are shown in Figure 9 for zero temperature (black) and T = 453.15 K (red), which is consistent with the experimental condition. We show results for the a-RS conformer (results are similar for the other conformers), Ph, and RV. Our calculations corroborate that H_2 elimination at low energies should not take place at the Ph subunit because the dissociation of the CH bonds is energetically less favorable compared to the polar OH bonds. On the other hand, the thresholds for H abstraction from Ph and a-RS are similar (though not discussed here, our results are consistent with the DEA data for Ph[14,41,42]). The present threshold estimates are generally in agreement with previous calculations.[11]

The formation of H_2 from RV, along with the *m*-benzoquinone (MBQ) anion, has a nearly zero threshold at 0 K, and the reaction becomes exothermic at higher temperatures. This is of course consistent with the formation H_2 at 0 eV. The calculated thresholds for H abstraction at 453 K are 0.3 eV (Ph subunit) and 0.5 eV (RS subunit). These estimates are also consistent with the observation of the $[M-H]^-$ fragment at 1.2 eV although not at 0 eV. Other fragments were observed at considerably higher energies (see Table 2), so they cannot be interpreted based on our calculations.

As stated above, one of the goals of our work was to investigate if the smaller RS molecule would be a prototype for the H_2-elimination reactions in RV. Molecular dynamics and reaction paths simulations would be considerably less demanding for the smaller system, apart from the advantages discussed above for the scattering computations (symmetry decomposition, dimension of CSF space, and polarization balance). While the formation of H_2 would also be exothermic in RS, the reaction should be suppressed by the absence of bound anion states. As stated above, the dipole moment magnitudes range from 1.4 to 2.5 D, depending on the isomer, and our calculations do not indicate a DBS for RS (if the DBS exists at all, it should be very shallow). In addition, the π_1^* state, which is bound in RV, becomes a resonance in RS, lying around 0.7 eV. Because there are not bound anion states, the observation of $[M-2H]^-$ fragments at 0 eV is not expected for RS. Our results are not in disagreement with the known antioxidant properties of RS because mechanisms not based on DEA have been pointed out.[17] The differences between RV

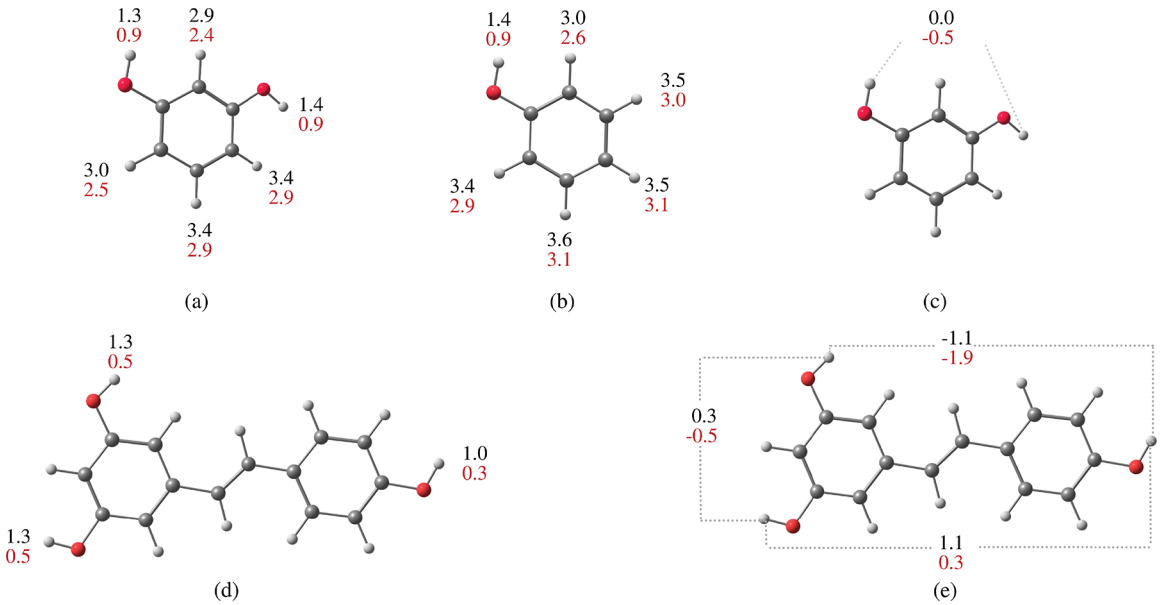

Figure 9. Free energy dissociation thresholds (in units of eV) obtained for (a) H abstraction from a-RS (a-RS + e^- → $[(a)\text{-RS}-H]^-$ + $H^\bullet$); (b) H abstraction from Ph (Ph + e^- → $[Ph-H]^-$ + H); (c) H_2 abstraction from a-RS (a-RS + e^- → $MBQ^{\bullet-}$ + H_2); (d) H abstraction from p-RV (p-RV + e^- → $[p\text{-RV}-H]^-$ + $H^\bullet$); and (e) H_2 abstraction from p-RV (p-RV + e^- → $[p\text{-RV}-2H]^{\bullet-}$ + H_2). The black and red numbers indicate respectively the thresholds at T = 0 and T = 453.15 K. The sites where the abstraction reactions take place are indicated by the position of the energy values in each panel.

https://doi.org/10.1021/acs.jpca.2c05789
J. Phys. Chem. A 2022, 126, 7667−7674

and RS actually suggest that the ethene and the Ph subunits play relevant roles in the H_2-elimination reaction, although an indirect one. Those subunits switch on the H_2-elimination mechanism in RV to the extent that they stabilize the π_1^* state.

CONCLUSIONS

We reported a theoretical investigation of the low-energy anion states of the polyphenolic compound RV. This is a challenging system for electron scattering calculations in view of its size and low symmetry. Even though description of correlation-polarization effects is not well balanced in our SEP results, our study provides a consistent interpretation of the previously reported DEA measurements. In addition to four shape resonances, our results point out a shallow valence bound state π_1^*. This anion state, along with the computed dissociation thresholds, supports that H_2 elimination at 0 eV would be initiated by π_1^*/σ_{OH}^* couplings. Because we could only converge a very shallow DBS for RV, we do not believe that H elimination at 0 eV is initiated by vibrational Feshbach resonances (VFRs) built on a DBS. The π_1^* state is also responsible for the formation of the parent M^- ion, also observed at 0 eV. The H-elimination reaction observed around 1.2 eV is triggered by two nearly degenerate shape resonances, π_3^* and π_4^*.

We also investigated the RS subunit, which could be a less computationally expensive prototype for the production of H_2, a reaction that could account for the antioxidant activity of RV, at least partly. We obtained two π^* shape resonances and a mixed-character resonance from SEP level scattering calculations. There is a correspondence between the anion states of RV and RS and even between the dissociation thresholds. However, the absence of bound anion states for the RS molecule is expected to suppress the H_2-formation channel at 0 eV. Our calculations therefore unveil the indirect part played by the ethene and Ph moieties of RV. They switch on the H_2-elimination mechanism initiated by π_1^*/σ_{OH}^* couplings because since they stabilize the π_1^* state.

ASSOCIATED CONTENT

Supporting Information

The Supporting Information is available free of charge at https://pubs.acs.org/doi/10.1021/acs.jpca.2c05789.

Additional content on the optimized geometries and the calculations of vertical excited states of the neutral targets (PDF)

AUTHOR INFORMATION

Corresponding Author

Márcio T. do N. Varella − *Instituto de Física, Universidade de São Paulo, 05508-090 São Paulo, São Paulo, Brazil;* orcid.org/0000-0002-5812-0342; Email: mvarella@if.usp.br

Authors

Ely G. F. de Miranda − *Instituto de Física, Universidade de São Paulo, 05508-090 São Paulo, São Paulo, Brazil*

Lucas M. Cornetta − *Instituto de Física Gleb Wataghin, Universidade Estadual de Campinas, 13083-859 Campinas, São Paulo, Brazil*

Complete contact information is available at: https://pubs.acs.org/10.1021/acs.jpca.2c05789

Notes

The authors declare no competing financial interest.

ACKNOWLEDGMENTS

E.G.F.M. acknowledges financial support from the São Paulo Research Foundation (FAPESP) under Grant 2021/09837-7 and Brazilian National Council for Scientific and Technological Development (CNPq) under Grant 131628/2019-4. L.M.C. acknowledges financial support from FAPESP under Grants 2020/04822-9 and 2021/06527-7. M.T.d.N.V. also acknowledges financial support from CNPq (Grant 304571/2018-0) and FAPESP (Grant 2020/16155-7). The calculations were partly performed with HPC resources from STI, University of São Paulo.

REFERENCES

(1) Metzler, D. The Chemical Reactions of Living Cells. *BioChem.* **1977**, 517−558.

(2) Ahmad, M.; Wolberg, A.; Kahwaji, C. I.*Biochemistry, Electron Transport Chain*; StatPearls Publishing: Treasure Island, FL, 2021.

(3) Pelster, L. N.; Minteer, S. D. Mitochondrial Inner Membrane Biomimic for the Investigation of Electron Transport Chain Supercomplex Bioelectrocatalysis. *ACS Catal.* **2016**, *6*, 4995−4999.

(4) Costa, R.; Romagna, C. D.; Pereira, J.; Souza-Pinto, N. C. The Role of Mitochondrial DNA Damage in the Cytotoxicity of Reactive Oxygen Species. *Journal of Bioenergetics and Biomembranes* **2011**, *43*, 25−29.

(5) Murphy, M. P. How Mitochondria Produce Reactive Oxygen Species. *Biochem. J.* **2009**, *417*, 1−13.

(6) Koopman, W. J.; Willems, P. H.; Smeitink, J. A. Monogenic Mitochondrial Disorders. *N. Engl. J. Med.* **2012**, *366*, 1132−1141.

(7) Andreyev, A. Y.; Kushnareva, Y. E.; Starkov, A. Mitochondrial Metabolism of Reactive Oxygen Species. *Biochemistry (Moscow)* **2005**, *70*, 200−214.

(8) Pshenichnyuk, S. A.; Modelli, A.; Komolov, A. S. Interconnections Between Dissociative Electron Attachment and Electron-Driven Biological Processes. *Int. Rev. Phys. Chem.* **2018**, *37*, 125−170.

(9) Modelli, A.; Pshenichnyuk, S. A. Gas-Phase Dissociative Electron Attachment to Flavonoids and Possible Similarities to their Metabolic Pathways. *Phys. Chem. Chem. Phys.* **2013**, *15*, 1588−1600.

(10) Ohsawa, I.; Ishikawa, M.; Takahashi, K.; Watanabe, M.; Nishimaki, K.; Yamagata, K.; Katsura, K.-i.; Katayama, Y.; Asoh, S.; Ohta, S. Hydrogen Acts as a Therapeutic Antioxidant by Selectively Reducing Cytotoxic Oxygen Radicals. *Nat. Med.* **2007**, *13*, 688.

(11) Pshenichnyuk, S. A.; Komolov, A. S. Dissociative Electron Attachment to Resveratrol as a Likely Pathway for Generation of the H_2 Antioxidant Species inside Mitochondria. *J. Phys. Chem. Lett.* **2015**, *6*, 1104−1110.

(12) Pshenichnyuk, S. A.; Komolov, A. S. Dissociative Electron Attachment to Anthralin to Model its Biochemical Reactions. *J. Phys. Chem. Lett.* **2014**, *5*, 2916−2921.

(13) Baur, J. A.; Sinclair, D. A. Therapeutic Potential of Resveratrol: The in vivo Evidence. *Nat. Rev. Drug Discovery* **2006**, *5*, 493.

(14) de Oliveira, E. M.; Sanchez, S. d.; Bettega, M. H.; Natalense, A. P.; Lima, M. A.; Varella, M. T. d. N. Shape Resonance Spectra of Lignin Subunits. *Phys. Rev. A: At., Mol., Opt. Phys.* **2012**, *86*, 020701.

(15) Szymańska, E.; Mason, N. J.; Krishnakumar, E.; Matias, C.; Mauracher, A.; Scheier, P.; Denifl, S. Dissociative Electron Attachment and Dipolar Dissociation in Ethylene. *Int. J. Mass Spectrom.* **2014**, *365*, 356−364.

(16) Arts, M. J.; Dallinga, J. S.; Voss, H.-P.; Haenen, G. R.; Bast, A. A Critical Appraisal of the Use of the Antioxidant Capacity (TEAC) Assay in Defining Optimal Antioxidant Structures. *Food Chem.* **2003**, *80*, 409−414.

(17) Ortega-Moo, C.; Garza, J.; Vargas, R. The Substituent Effect on the Antioxidant Capacity of Catechols and Resorcinols. *Theor. Chem. Acc.* **2016**, *135*, 1−12.
(18) Frisch, M. J.; et al.*Gaussian09*, Revision E.01; Gaussian Inc.: Wallingford, CT, 2009.
(19) Tsuzuki, S.; Honda, K.; Uchimaru, T.; Mikami, M.; Tanabe, K. Origin of attraction and directionality of the π/π interaction: model chemistry calculations of benzene dimer interaction. *J. Am. Chem. Soc.* **2002**, *124*, 104−112.
(20) Hwang, J.; Dial, B. E.; Li, P.; Kozik, M. E.; Smith, M. D.; Shimizu, K. D. How Important Are Dispersion Interactions to the Strength of Aromatic Stacking Interactions in Solution? *Chem. Sci.* **2015**, *6*, 4358−4364.
(21) Winstead, C.; McKoy, V. Interaction of Low-Energy Electrons with the Purine Bases, Nucleosides, and Nucleotides of DNA. *J. Chem. Phys.* **2006**, *125*, 244302.
(22) Dora, A.; Bryjko, L.; van Mourik, T.; Tennyson, J. Low-Energy Electron Scattering with the Purine Bases of DNA/RNA using the R-matrix Method. *J. Chem. Phys.* **2012**, *136*, 024324.
(23) Nunes, F.; Varella, M.; Pastega, D. F.; Freitas, T.; Aurélio Pinheiro Lima, M.; Bettega, M.; Sanchez, S. Transient Negative Ion Spectrum of the Cytosine-Guanine Pair. *Eur. Phys. J. D* **2017**, 71.
(24) Scheer, A. M.; Burrow, P. D. π^* Orbital System of Alternating Phenyl and Ethynyl Groups: Measurements and Calculations. *J. Phys. Chem. B* **2006**, *110*, 17751−17756.
(25) Santos, J. S. d.; da Costa, R. F.; Varella, M. T. d. N. Low-Energy Electron Collisions with Glycine. *J. Chem. Phys.* **2012**, *136*, 084307.
(26) Bettega, M.; Ferreira, L.; Lima, M. Transferability of Local-Density Norm-Conserving Pseudopotentials to Electron-Molecule-Collision Calculations. *Phys. Rev. A: At., Mol., Opt. Phys.* **1993**, *47*, 1111.
(27) da Costa, R. F.; Varella, M. T. d. N.; Bettega, M. H.; Lima, M. A. Recent Advances in the Application of the Schwinger Multichannel Method with Pseudopotentials to Electron-Molecule Collisions. *Eur. Phys. J. D* **2015**, *69*, 1−24.
(28) Joachain, C.*Quantum Collision Theory*; North-Holland Publishing Company: 1975.
(29) Bachelet, G.; Hamann, D.; Schlüter, M. Pseudopotentials that Work: From H to Pu. *Phys. Rev. B: Condens. Matter Mater. Phys.* **1982**, *26*, 4199.
(30) Dunning, T. H., Jr. Gaussian Basis Functions for Use in Molecular Calculations. I. Contraction of (9s5p) Atomic Basis Sets for the First-Row Atoms. *J. Chem. Phys.* **1970**, *53*, 2823−2833.
(31) Barca, G. M. J.; et al. Recent Developments in the General Atomic and Molecular Electronic Structure System. *J. Chem. Phys.* **2020**, *152*, 154102.
(32) Kossoski, F.; Bettega, M. Low-Energy Electron Scattering from the Aza-Derivatives of Pyrrole, Furan, and Thiophene. *J. Chem. Phys.* **2013**, *138*, 234311.
(33) Bauschlicher, C. W., Jr. The Construction of Modified Virtual Orbitals (MVO's) which are Suited for Configuration Interaction Calculations. *J. Chem. Phys.* **1980**, *72*, 880−885.
(34) Roos, B. O.; Andersson, K.; Fülscher, M. P.; Serrano-Andrés, L.; Pierloot, K.; Merchán, M.; Molina, V. Applications of Level Shift Corrected Perturbation Theory in Electronic Spectroscopy. *J. Mol. Struct.: THEOCHEM* **1996**, *388*, 257−276.
(35) Fdez. Galvan, I.; Vacher, M.; Alavi, A.; Angeli, C.; Aquilante, F.; Autschbach, J.; Bao, J. J.; Bokarev, S. I.; Bogdanov, N. A.; Carlson, R. K.; et al. OpenMolcas: From Source Code to Insight. *J. Chem. Theory Comput.* **2019**, *15*, 5925−5964.
(36) Curtiss, L. A.; Redfern, P. C.; Raghavachari, K. Gaussian-4 Theory using Reduced Order Perturbation Theory. *J. Chem. Phys.* **2007**, *127*, 124105.
(37) Cornetta, L.; Kossoski, F.; Varella, M. d. N. Transient Anion Spectra of the Potential Radiosensitizers 5-Cyanateuracil and 5-Thiocyanateuracil. *J. Chem. Phys.* **2017**, *147*, 214310.
(38) Kossoski, F.; Bettega, M.; Varella, M. d. N. Shape Resonance Spectra of Uracil, 5-Fluorouracil, and 5-Chlorouracil. *J. Chem. Phys.* **2014**, *140*, 024317.
(39) Skurski, P.; Gutowski, M.; Simons, J. How to Choose a One-Electron Basis Set to Reliably Describe a Dipole-Bound Anion. *Int. J. Quantum Chem.* **2000**, *80*, 1024−1038.
(40) Burrow, P.; Gallup, G. A.; Scheer, A. M.; Denifl, S.; Ptasinska, S.; Märk, T.; Scheier, P. Vibrational Feshbach Resonances in Uracil and Thymine. *J. Chem. Phys.* **2006**, *124*, 124310.
(41) Jordan, K.; Michejda, J.; Burrow, P. Electron Transmission Studies of the Negative Ion States of Substituted Benzenes in the Gas Phase. *J. Am. Chem. Soc.* **1976**, *98*, 7189−7191.
(42) Khatymov, R. V.; Muftakhov, M. V.; Mazunov, V. A. Phenol, Chlorobenzene and Chlorophenol Isomers: Resonant States and Dissociative Electron Attachment. *Rapid Commun. Mass Spectrom.* **2003**, *17*, 2327−2336.

https://doi.org/10.1021/acs.jpca.2c05789
J. Phys. Chem. A 2022, 126, 7667−7674